Integrated Photonic Devices and Materials Group

Academic and Research Staff
Professor Leslie A. Kolodziejski, Dr. Gale S. Petrich, Principal Research Scientist

Graduate Students
Solomon Assefa, Reginald E. Bryant, Yamini Kangude, Aleksandra Markina, Eric Mattson, Sarah J. Rodriguez, Sheila N. Tandon, and Ryan D. Williams

Technical and Support Staff
Jacques L. Wood

Introduction

The emphasis of our research program is the design, epitaxial growth, device fabrication and characterization of a number of photonic and opto-electronic structures and devices. The epitaxial growth of the heterostructures is performed in the laboratory consisting of two gaseous source epitaxy reactors interconnected to several smaller chambers, which are used for sample introduction and in-situ surface analysis.

The laboratory has purchased a Veeco GEN 200 solid source, dual-reactor molecular beam epitaxy system. The new system will allow for the epitaxial growth of dilute nitrides and antimony-based films in addition to arsenide- and phosphide-based films. The system platens hold multiple 3" or 4" wafers, or a single 6" or 8" wafer. The system incorporates a low wobble manipulator that will enable in-situ feedback control of the epitaxial processes using optical sensors such as band edge absorption and spectroscopic ellipsometry. The system is currently awaiting the completion of the new laboratory at MIT to begin the installation of the epitaxy tool.

In the following sections, the status of the various research projects will be discussed. The existing III-V gas source molecular beam epitaxy system is utilized for the development of GaAs-based tunnel-junction-coupled lasers, for the fabrication of GaAs-based devices implementing one- and two-dimensional photonic bandgap crystals within their structure, for the development of components for ultra short pulse lasers, and for the development of electromechanical optical switches. The development of tunnel-junction-coupled lasers represents a collaboration between the research groups of Prof. Rajeev Ram and Prof. Leslie Kolodziejski. The research projects utilizing photonic crystals in addition to the development of the optical switch represents the combined efforts of the research groups led by Professors John D. Joannopoulos (Theory), Leslie A. Kolodziejski (Fabrication), Henry I. Smith (Fabrication), and Erich P. Ippen (Measurement). The complexity of the design, fabrication and characterization of these photonic crystal-based structures necessitates a strong interaction between the various research groups. A collaborative effort between the groups led by Professors Kolodziejski, Ippen and Kaertner has led to the development of saturable bragg reflectors that are required in ultra short pulse lasers.

1. Quantum Dot Laser Research

Sponsors
DARPA/Brown University: Sub Award #1123-24596

Project Staff
Ryan D. Williams, Dr. Gale S. Petrich, Professor Rajeev Ram and Professor Leslie A. Kolodziejski

The tunnel-junction-coupled laser design aims to combine two or more lasing active regions in epitaxial series. Previous work realized operable tunnel-junction-coupled lasers at 980 nm. The original 980 nm quantum well based design has been adapted for 1300 nm quantum dot based design. In addition, the electrical performance of the reverse-biased tunnel junction which connects consecutive active regions epitaxially has been measured.

As 1300 nm is an important communications wavelength, recent work has focused on obtaining InAs quantum dots on GaAs substrates. The use of InAs quantum dots extend the emission range of GaAs-based active regions well into the functional telecommunications wavelengths. Furthermore, quantum dots allow for the realization of ultra-low laser threshold currents, narrow emission spectra, improved gain properties, and increased temperature stability. Photoluminescence studies have shown strong emission between 1250-1300 nm. Careful control of the growth conditions, such as the substrate temperature and deposition rate have allowed precise control over the emission wavelength and intensity. Atomic force microscopy has been used to confirm the presence of quantum dots and has shown their average diameter to be around 20 nm.

The introduction of indium into the GaAs tunnel junction material is theorized to improve the differential resistance of the junction and thereby increase the tunneling current, resulting in improved quantum efficiency for the laser. Samples have been grown by gas source molecular beam epitaxy and processed to examine the effects of indium-incorporation. Electrical testing confirms a correlation between higher indium content (smaller bandgap) and larger tunneling currents.

Tunnel-junction-coupled laser structures with active regions composed of quantum wells emitting at 980 nm and quantum dots emitting at 1300 nm have been deposited. An oxide stripe laser process has been developed and implemented. Complete lasers were fabricated and characterized using electroluminescence. Future work hopes to improve the fabrication process to allow for further testing and characterization of the lasers.

2. Towards Optical Logic: Integration Scheme

Sponsors
Lincoln Laboratory: Contract Number BX-008506

Project Staff
Aleksandra Markina, Sarah J. Rodriguez, Dr. Gale S. Petrich, Professor Leslie A. Kolodziejski, and Dr. Scott Hamilton

The goal of this project is to create the technology for the design, simulation and fabrication of an Optical Logic Unit Cell composed of semiconductor optical amplifiers (SOAs) embedded within a Mach Zehnder interferometer. By integrating one SOA into each arm of the interferometer, and by controlling how the optical signal is coupled to the Mach Zehnder, various logic functions such as AND, NAND, and XOR can be implemented.

Monolithic integration of semiconductor optical devices requires fabrication of low-loss interconnects between the active devices and the passive waveguides. For this project, the twin waveguide approach was chosen for the monolithic integration of SOAs with passive components. The chief advantage of this approach is that it provides low-loss, efficient optical coupling without the need for epitaxial regrowth as post-growth patterning and fabrication defines all the integrated components. The greatest challenge is the need for sub-micron lithography and precise alignment of the active waveguide taper to the passive waveguide.

In the twin waveguide (TG) design, two strongly coupled waveguides are stacked vertically, separated by a cladding layer. The active waveguide typically resides on top of a passive waveguide. In an asymmetric TG (ATG) structure, one of the modes is largely confined to the active guide and the other mode is primarily confined to the passive guide. Introduction of a lateral taper within the active waveguide drastically reduces the coupling loss and improves the quality of twin-waveguide. Tapers also have been demonstrated to have extremely low reflection, making them an excellent choice for the SOA design. The tapered active waveguide has a higher index of refraction than the lower transparent waveguide. The light confined in the passive waveguide is adiabatically coupled to the active waveguide [1], [2].

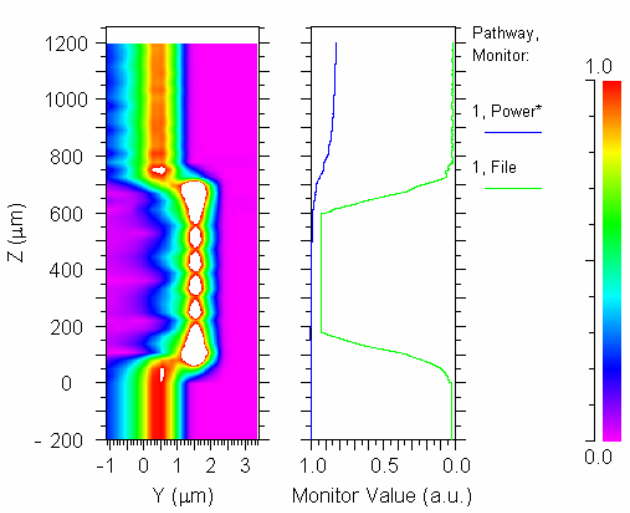

Figure 1. Optical power transfer in a twin waveguide structure.

A number of parameters need to be optimized in order to reduce coupling losses in twin waveguides. The first group of parameters concerns the layer composition of the TG. The lower waveguide needs to have a low index of refraction, which can be achieved with the use of dilute waveguides. Thickness of the InP cladding layer between the two waveguides and the InP cap layer on top of the active waveguide requires optimization. In lateral dimensions, the taper length and starting width can be varied to improve the optical coupling. Figure 1 shows total optical power and the power in the fundamental mode of the twin waveguides structure with an active waveguide that is 425 microns long.

3. Towards Optical Logic: Optical Wires

Sponsors:
Lincoln Laboratory: Contract Number BX-008506
Army Research Office, Contract Number DAAD19-03-1-0090

Project Staff: Sarah J. Rodriguez, Aleksandra Markina, Dr. Gale S. Petrich, Professor Leslie A. Kolodziejski

Photonic integrated circuits allow the miniaturization of discrete optical subsystems currently used in the telecommunications industry. Photonic integrated circuits may comprise a number of devices including semiconductor optical amplifiers, optical pulse generators, polarization splitters and phase shifters to name a few. All of these devices will be integrated with the use of waveguides. One of the major design issues associated with waveguides is the amount of space used for the waveguide bends. While tighter bends require less space, they are more prone to radiation loss. Finding a low loss solution to the issue of waveguide bending is essential in reducing the overall die size.

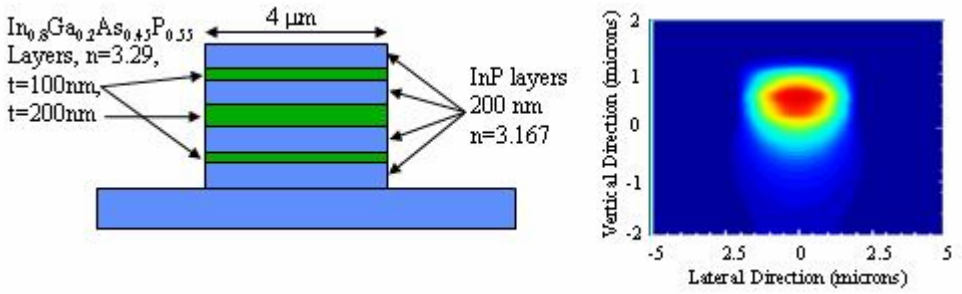

Figure 2. Dilute waveguide design and its mode profile.

The goal in this project is to fabricate and optically characterize waveguide bends in the (In,Ga)(As,P) material system for use in photonic integrated circuits. (In,Ga)(As,P) heterostructures have been grown by gas source molecular beam epitaxy on InP substrates. To minimize material and coupling losses, a dilute waveguide with a low effective index is implemented and may be obtained by alternating quaternary ($In_{0.56}Ga_{0.44}As_{0.95}P_{0.07}$, n=3.294) layers with InP layers (n=3.17). Figure 2 depicts the as-grown structure accompanied by its mode profile.

A mask was designed containing seventeen six by six millimeters dies [Figure 3(a)]. All the dies consist of straight waveguides followed by a set of three identical waveguides containing a number of bends; Figure 3(b) depicts an example of a die. For each bend radius, there are three sets of three identical waveguides. Each set contains a different number of bends. Hence, by using a linear regression, the loss per bend can be determined. Each bend is matched with its mirror image (y-axis), to ensure that the entry and the exit points lay on the same line, for ease in measuring. The widths of the waveguides in dies A through P vary from 1 micron to 7 microns. Die Q contains resonator bends.

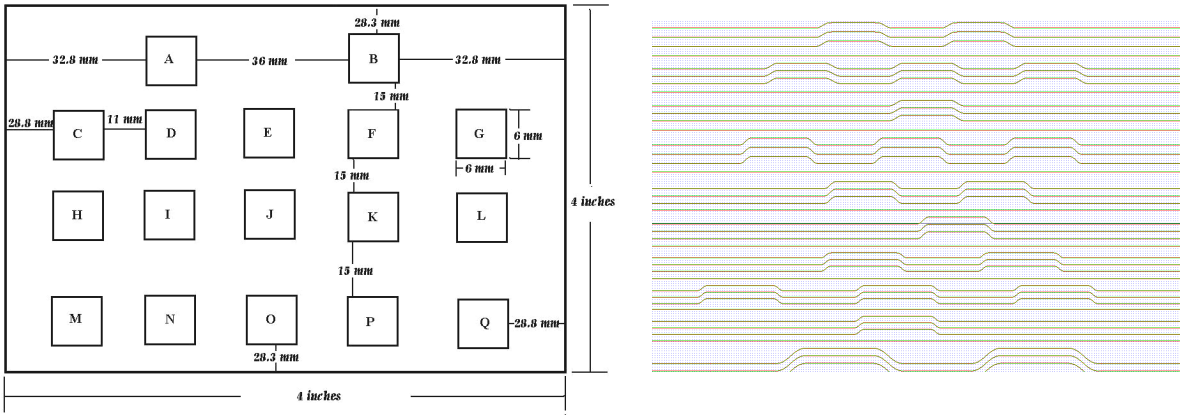

Figure 3. a) The layout of the dies. b) Within each die, the radius of curvature and the number of bends per waveguide are varied.

The fabrication process includes the gas source molecular beam epitaxy growth of the heterostructure on an InP substrate, the deposition of a $Si0_2$ hard mask layer, photolithography and reactive ion etching. Figure 4 shows a scanning-electron beam micrograph of a waveguide bend of a dilute waveguide structure. Waveguides are currently being tested.

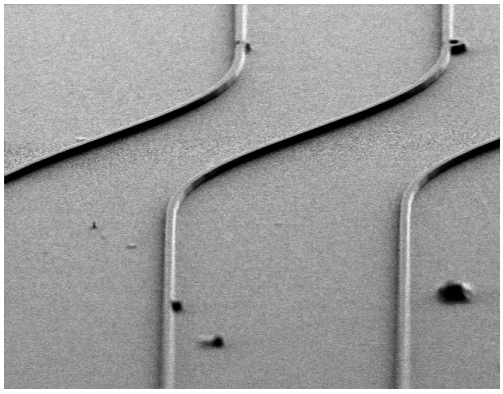

Figure 4. Curved ridge waveguides composed of InGaAsP and InP layers on an InP substrate with a 146nm thick SiO_2 etch mask. The epilayers have been etched to a depth of 1.56 microns.

4. Coupling into Photonic Crystal Waveguides

Sponsors:
National Science Foundation Award Number DMR-02-13282

Project Staff:

Solomon Assefa, Peter Rakich, Dr. Peter Bienstman, Dr. Steven G. Johnson, Dr. Gale S. Petrich, Professor John D. Joannopoulos, Professor Leslie A. Kolodziejski, Professor Erich P. Ippen, and Professor Henry I. Smith

Large-scale photonic integrated circuits require guiding light around sharp bends with a radius of curvature on the order of a wavelength. In conventional index-guided waveguides, light is confined as a result of total internal reflection at the interface between the high refractive index waveguiding layer and the low index surroundings. However, using these conventional waveguides in photonic integrated circuits would be difficult because they are susceptible to large optical losses as the bend's radius of curvature decreases. Photonic crystals (PCs), which consists of a periodic arrangement of high and low-index dielectric material, have been proposed as a potential solution in order to guide light around corners including 90^{o} bends with near perfect transmission.

The 2D photonic crystal under investigation consists of an array of cylindrical rods of high dielectric material residing on a low dielectric constant material. Introducing a line defect, such as a row of smaller radius cylinders into the 2D photonic crystal, results in a linear waveguide (Figure 5). The arrangement of periodic dielectric rods surrounding the line defect creates a photonic band gap (PBG), i.e. a range of frequencies in which light can not propagate. Thus, an optical signal with a frequency inside the PBG has its energy confined within the line defect and becomes evanescent in the photonic crystal. The radius of the cylinders in the line defect remains large enough to provide index guiding in the third dimension (normal to the plane of periodicity). The localization of a mode inside the line defect can be utilized to guide light around sharp corners including a 90^{o} bend with low optical loss.

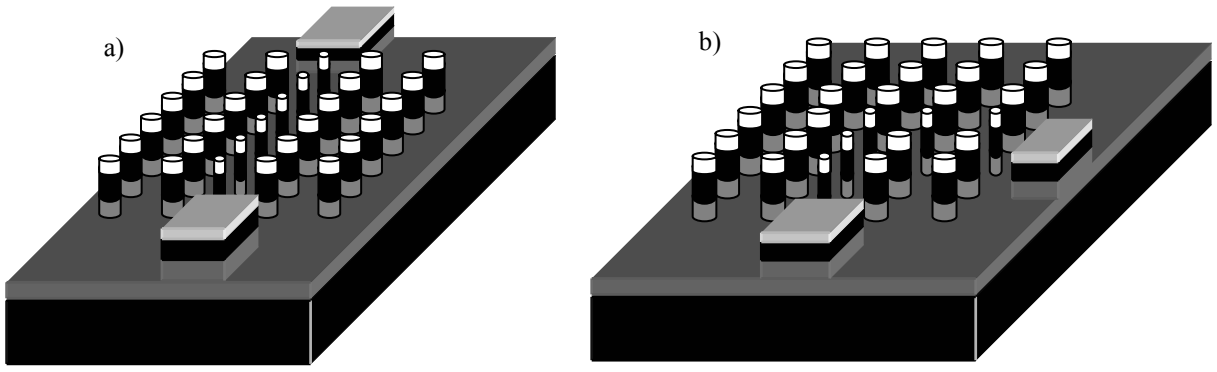

Figure 5. (a) Schematic of a linear PC waveguide. (b) Schematic of a 90^{o}-bend PC waveguide.

Nevertheless, the practical use of photonic crystal waveguides is limited due to the poor coupling efficiency between photonic crystal waveguides, and conventional index-guided waveguides. Coupling between waveguides poses a challenge because the photonic crystal waveguide exhibits a significantly different mode profile and propagation mechanism as compared to traditional waveguides that use index confinement. In a conventional waveguide, the optical field has only forward propagating components, while the field in the photonic crystal waveguide has both forward and backward propagating components due to scattering. Furthermore, in conventional waveguides, light is guided within high index material that is surrounded by low index material; in the photonic crystal waveguide, light is guided within low index material that is surrounded by two photonic crystal mirrors.

Figure 6 compares three different designs for coupling light into the line defect photonic crystal waveguide. The design in Figure 6(a) suffers from Fabry-Perot reflection at the edges of the photonic crystal region, which makes the transmission of the waveguide dependent on the waveguide length. By tapering the end of the input and output index waveguides, as shown in Figure 6(b), Fabry-Perot reflections can be somewhat reduced. In the third design, the input waveguide is adiabatically converted into a strongly coupled-cavity waveguide. The coupling scheme adiabatically transforms the forward propagating component of the field into both forward and backward propagating components before reaching the photonic crystal. Also, the photonic crystal cladding is introduced slowly from the edge, thereby adiabatically transforming the mode from high-index guiding to bandgap guiding. Two-dimensional simulations show that this coupling scheme results in nearly 100% transmission through the photonic crystal waveguide.

The cylindrical rods of the photonic crystal consist of a 550nm thick high-index epitaxial GaAs layer and an 800nm thick low-index Al_xO_y layer. An additional 600nm thick Al_xO_y spacer layer resides below the cylindrical rods isolating the GaAs guiding layer from the GaAs substrate. The heterostructure is grown using gas source molecular beam epitaxy on a GaAs (100) substrate. The Al_xO_y is initially grown epitaxially as $Al_{0.9}Ga_{0.1}As$ and is subsequently thermally oxidized.

The fabrication process commences by sputter deposition of a 300nm thick layer of SiO_2 on the sample. Next, the waveguide and photonic crystal are defined using direct-write electron-beam lithography. Each sample is coated with polymethylmethacrylate (PMMA) electron beam resist, and each cylinder is defined by exposing a square pattern. The finite width of the beam rounds-off the corners of each square yielding a circular hole upon development. Simulations show that the largest bandgap is obtained from a periodic arrangement of rods with a diameter of 300nm. The input and output coupling waveguides and different sized arrays of holes are electron-beam-written by stitching together 250μm size fields. A 40nm thick nickel film is evaporated on the sample after the PMMA is developed, and a liftoff process is performed. The pattern is transferred to the SiO_2 by reactive-ion etching (RIE) in a CHF_3 plasma after which the nickel mask is removed using nickel etchant. Using the SiO_2 mask, the cylindrical rods are created by etching the GaAs and the AlGaAs to a total depth of 1.5 μm using a BCl_3/He plasma. Next, each sample is cleaved in order to create a smooth input facet to promote the efficient coupling of an optical test signal with a wavelength of 1.55 μm. The AlGaAs is transformed into Al_xO_y using a wet thermal oxidation process.

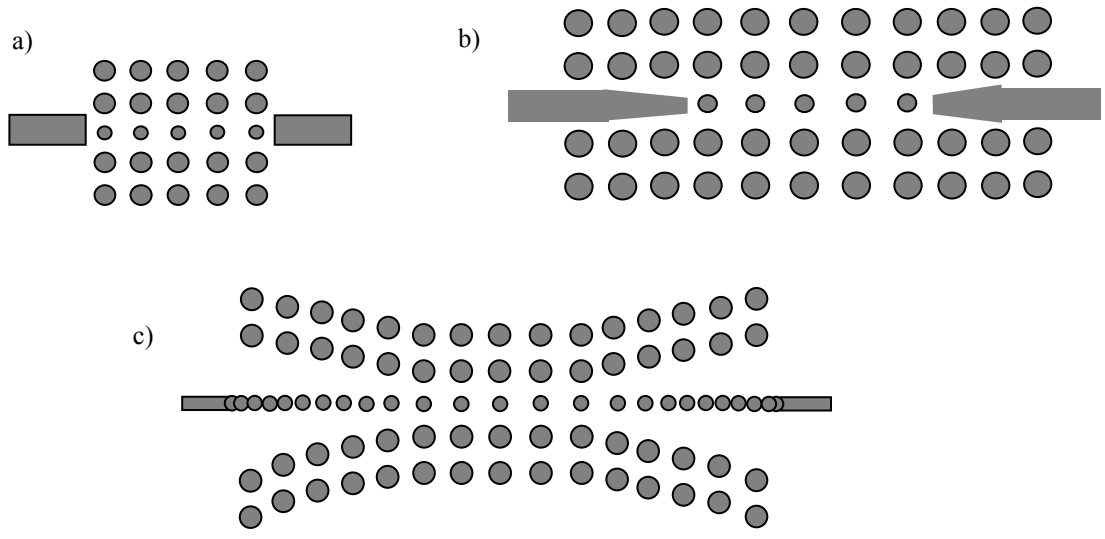

Figure 6. Schematic diagrams of coupling (a) from an untapered dielectric waveguide, (b) from a tapered dielectric waveguide, (c) using an adiabatic transition from a dielectric waveguide into strongly coupled cavities and tapered photonic crystal cladding.

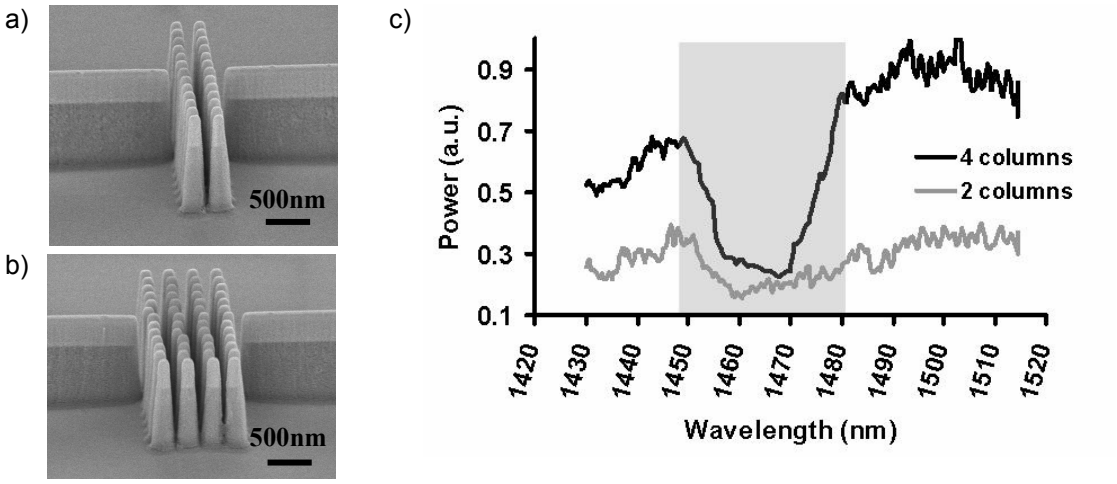

Figure 7. (a) Scanning Electron Micrograph (SEM) image of photonic crystal with two columns of dielectric pillars (b) SEM image of a photonic crystal with four columns of dielectric pillars (c) Transmission measurements through the two structures.

To optically characterize the devices, light is launched into the GaAs waveguide using a fiber and input coupler; the signal from the output is analyzed with a photodiode. The transmission measured through the bulk photonic crystal with a bandgap of 1448 to 1482 nm is shown in Figure 7. Employing the two-stage coupling scheme, the transmission versus wavelength for the photonic crystal waveguide is shown in Figure. 8. The measured result demonstrates bandgap guiding of light within a photonic crystal waveguide. Currently, the various types of bends illustrated in Figure 9 are under investigation

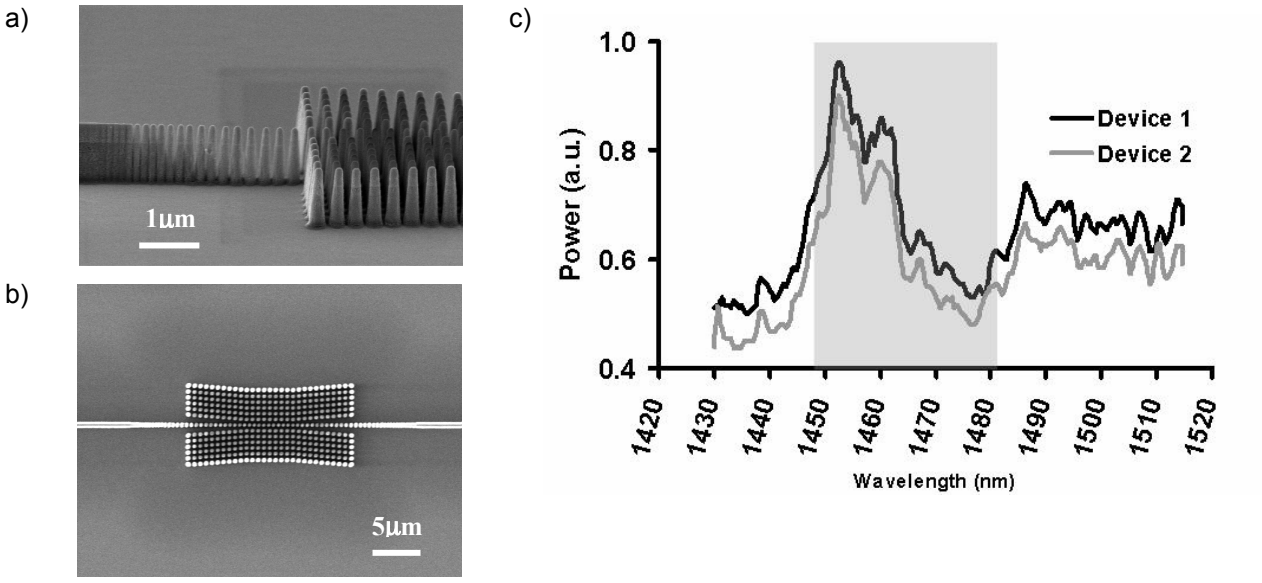

Figure 8. (a) Top-down SEM image of tapered photonic crystal waveguide (b) Side view SEM image of tapered photonic crystal waveguide. (c) Transmission measurement through the structures in (a) and (b). Two PC waveguides fabricated on the same chip demonstrated similar transmission.

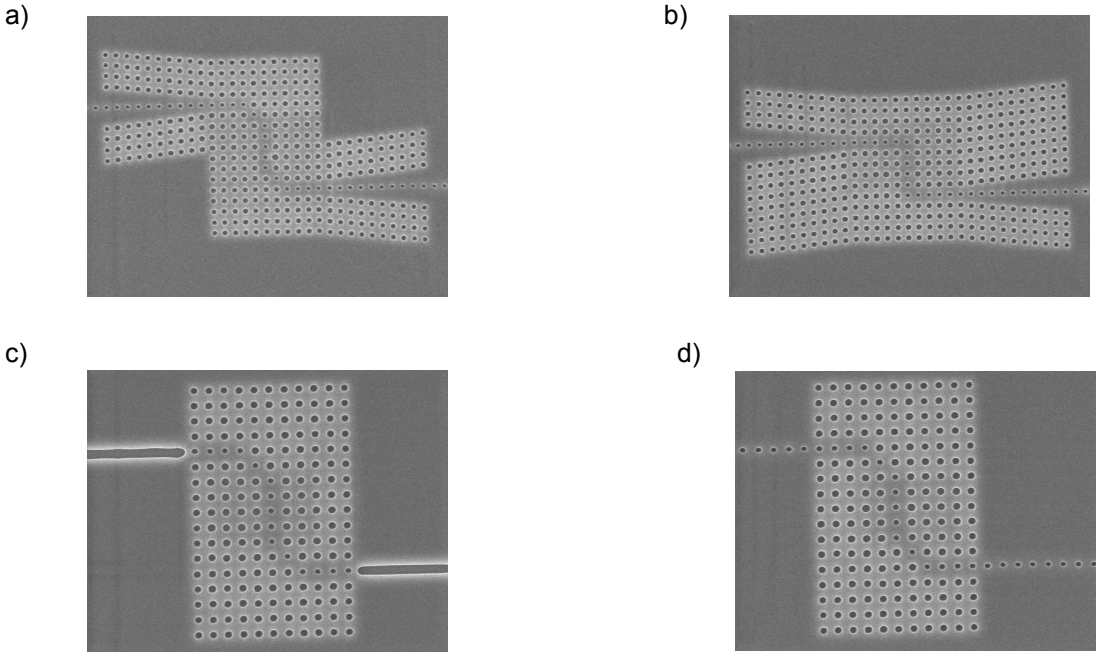

Figure 9. SEM images of sharp-bend waveguides after PMMA e-beam exposure and development.

5. Oxidation of AlAs Layers for Large-Area Broadband Saturable Bragg Reflectors from the Infrared to Visible

Project Staff:
Sheila N. Tandon, Juliet T. Gopinath, Hanfei M. Shen, Dr. Gale S. Petrich, Prof. Leslie A. Kolodziejski, Prof. Franz X. Kaertner, and Prof. Erich P. Ippen

Sponsor
National Science Foundation, Award Number ECS-0322740
Office of Naval Research, Contract Number N00014-02-1-0717

AlAs/GaAs or AlAs/AlGaAs mirrors with saturable absorbers have limited bandwidth due to the low index-contrast of the materials. Thus, these mirrors are not suitable for broadband applications such as ultra-short pulse lasers. In an effort to improve the mirror's bandwidth, semiconductor absorbers have been transferred onto broadband metal mirrors by post-processing [3]. In addition, a broadband Saturable Bragg Reflector (SBR) with an epitaxially-grown AlGaAs/CaF_2 mirror and a GaAs absorber has been demonstrated with a Ti:Sapphire laser [4]. An alternative is to monolithically integrate absorbers onto Bragg-mirrors and use steam oxidation to convert AlAs layers to lower index Al_xO_y (n~1.6). The absorber and high index layers are selected based on the laser's wavelength. AlGaAs/Al_xO_y mirrors with InGaAs absorbers form large area broadband SBRs for infrared lasers, including Cr:Forsterite [5]. When thicker absorbers are used to increase the saturable loss, the strain from the InGaAs-based absorber results in absorber delamination during AlAs oxidation. Varying the temperature profile before and after oxidation stabilizes the structure. For visible wavelengths, SBRs are fabricated with InGaAlP high-index layers and GaAs absorbers. Using these oxidation techniques, SBRs with broadband reflectivities are created for lasers from the visible to infrared (Figure 10).

SBR epilayers were grown using gas source molecular beam epitaxy on GaAs. SBRs were defined using photolithography and wet etchants, and subsequently oxidized in a tube furnace at temperatures from 400-435°C. To examine the extent of oxidation, cross-sectional images were obtained using scanning

electron microscopy (SEM). Reflectivity measurements were obtained using Fourier-transform infrared (FTIR) spectroscopy and a microspectrophotometer. Pre-oxidation thicknesses were determined from FTIR spectroscopy and high-resolution x-ray diffraction rocking curves of unoxidized SBRs.

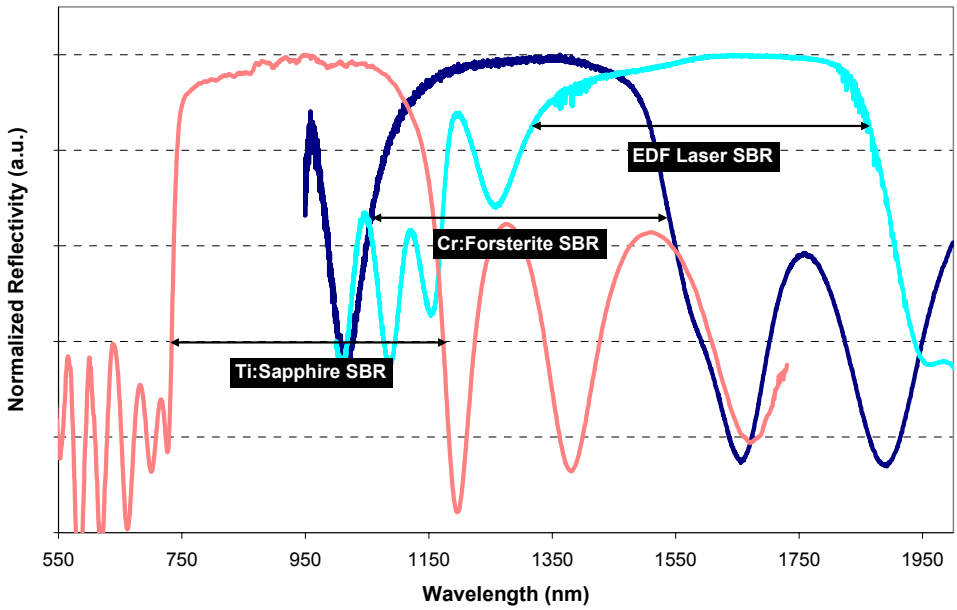

Figure 10. Reflectivity measurements of SBR structures fabricated for three different laser systems: Ti:Sapphire, Cr:Forsterite, and Er-doped fiber (EDF) laser with theoretical mirror reflectivity > 99% over 294nm, 466nm, and 563nm, respectively. The Ti:Sapphire SBR was measured with a microspectrophotometer (courtesy of Filmetrics, Inc.). SBRs for the Cr:Forsterite and EDF lasers were measured using FTIR. All measurements reveal losses due to SBR absorption.

Figure 11(a) shows plan and cross-sectional views of one SBR design for a center wavelength of 1230nm. The top view shows a fully-oxidized 500μm diameter SBR. The large diameter helps counteract two-photon absorption. The cross-section [Figure 11(b)] shows the delaminated absorber consisting of a highly strained 80nm InGaAs quantum well with GaAs cladding layers, and a 7-pair $Al_{0.3}Ga_{0.7}As/Al_xO_y$ mirror stack. For oxidations temperatures between 410°C and 435°C, delamination along the cleavage plane occurs between the absorber and mirror layers. More severe delamination occurs at higher oxidation temperatures. Lower epitaxial growth temperatures improve the absorber's stability upon oxidation. However, in an alternate SBR design, additional strain introduced by the InP cladding layers resulted in delamination despite lower growth temperatures. A controlled temperature ramp before and after oxidation has greatly reduced delamination for SBR structures grown at both temperatures [Figure 11(c)]. The oxidation temperature ramp allows for the creation of large area, broadband SBRs with highly-strained absorbers for lasers in the infrared including an Er-doped fiber laser [6].

The large scale oxidation technique also enables the fabrication of broadband SBRs at visible wavelengths. $In_{0.5}Ga_{0.15}Al_{0.35}P$, with a bandgap at 536nm and index of ~3.1, is lattice-matched to GaAs and is used as the high-index layer. With low-index Al_xO_y layers, mirrors are created for broadband reflection below 800nm. The top and side views of one structure are shown in Figure 12. With a GaAs absorber layer, the structure is nominally unstrained and will be able to modelock a variety of lasers including Ti:Sapphire, Cr:LiSAF, Cr:LiCAF, and Cr:LiSGaF.

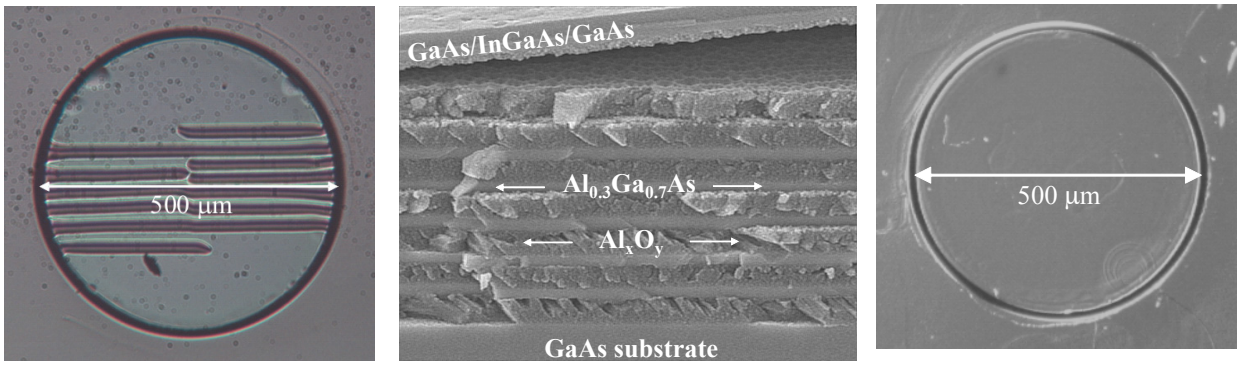

(a) (b) (c)

Figure 11. (a) Differential Interference Contrast (DIC) image of fully-oxidized SBR (420°C, 3.5hrs). (b) SEM image of SBR cross-section showing delamination of absorber layers: 52nm GaAs/80nm InGaAs/52nm GaAs with 7 pair $Al_xO_y/Al_{0.3}Ga_{0.7}As$ mirror stack (~194nm/100nm). (c) DIC image of SBR fully-oxidized using 50min temperature ramp between 100°C and 410°C before and after oxidation (410°C, 4.5hrs).

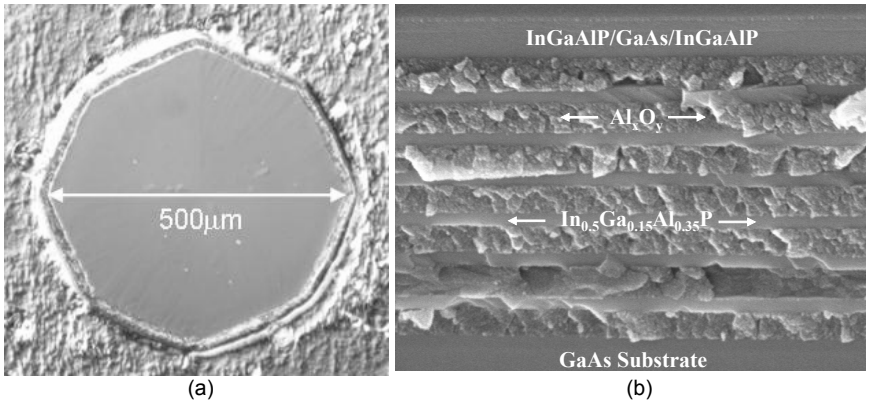

(a) (b)

Figure 12. (a) Differential Interference Contrast (DIC) image of fully-oxidized SBR (410°C, 4.5hrs with temperature ramp). (b) SEM image of SBR cross-section showing 60 nm $In_{0.5}Ga_{0.15}Al_{0.35}P$, 10nm GaAs, 60 nm $In_{0.5}Ga_{0.15}Al_{0.35}P$ absorber with a 7 pair $In_{0.5}Ga_{0.15}Al_{0.35}P/Al_xO_y$ mirror stack (65nm/~135nm).

6. Design and Fabrication of a Superprism Using Two Dimensional Photonic Crystals

Project Staff

Sheila N. Tandon, Chiyan Luo, Dr. Marin Soljacic, Dr. Gale S. Petrich, Professor John D. Joannopoulos, Professor Henry I. Smith and Professor Leslie A. Kolodziejski

Sponsor

Rockwell Science Center: Contract Number B1F431652

A superprism is an optical device similar to a conventional prism only with two enhanced properties: (1) super-dispersion and (2) ultra-refraction. Just as a conventional prism separates light into multiple wavelengths, a superprism separates these wavelengths over wider angles--termed “super-dispersion.” A superprism can also be used to magnify the angle of propagation of a single wavelength of light to steer the beam over wide angles--termed “ultra-refraction.” Photonic crystals form the essence of the

superprism effect. Being able to realize these superprism effects would be very useful for a number of applications ranging from enhanced devices for wavelength division multiplexed (WDM) systems to a new class of ultra-refractive optical elements for beam manipulation.

The device consists of a 2D photonic crystal with a square lattice of cylindrical air holes in a high index material such as silicon or gallium arsenide. The top view schematic of the device shape is shown in Figure 13. The device is hexagonal shaped with the photonic crystal (PC) occupying a square region in the middle. The initial design has focused on realizing ultra-refraction such that an input angular sweep of approximately +/- 2 degrees is amplified to about +/- 30 degrees at the output for a wavelength of 3.2 μm. A thick low index layer is used to minimize radiation loss into the high index substrate.

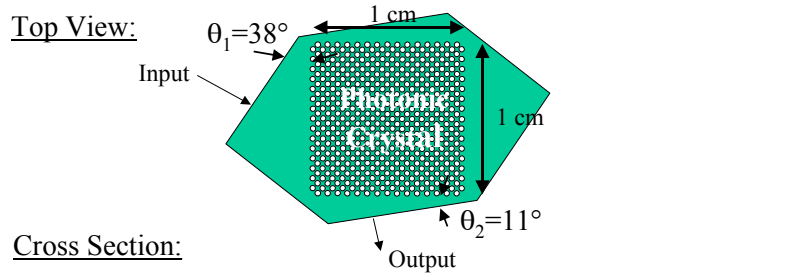

	GaAs Substrate		Si Substrate	
	λ=~3.1 μm	*λ=~1.55 μm*	*λ=~3.1 μm*	*λ=~1.55 μm*
PBG Lattice Constant	750 nm	372 nm	750 nm	372 nm
PBG Hole Radius	300 nm	150 nm	300 nm	150 nm
High Index Thickness	450 nm	223 nm	700 nm	205 nm
Low Index Thickness	3000 nm	1500 nm	3000 nm	3000 nm

Figure 13. Superprism device design showing schematic top and side views of the device.

The feature sizes of the photonic crystal can be scaled depending on the wavelength of operation as shown in Figure 13. The desired wavelengths of 3.1μm and 1.55μm imply hole lattice constants of 750nm and 372nm, and hole radii of 300nm and 150nm. The total thickness of the device (excluding substrate) is about 3.5 microns (460nm GaAs, 3μm Al_xO_y) while the top surface will have an area of about 2x2cm.

The hexagonal device shape is patterned using photolithography while the photonic crystal holes are patterned using interference lithography. After each lithography step, patterns are etched into the hard mask layers via reactive ion etching (RIE). The fully patterned hard mask layers are then used to etch the substrate material via another RIE step.

The full device is shown, in Figure 14, with its input and output facets shown in part (a). The photonic crystal occupies the square region and in Figure 14(b), a magnified plan-view of the corner area is shown. Figure 14(b) illustrates that very high alignment accuracy was achieved during the interference lithography step so that a line of holes was aligned to the square region with an error less than 1°. Figure 14(c) shows an SEM micrograph of the cross-section of a silicon monitor sample that was processed in parallel with the fabricated device. The cross-section shows the air holes that are etched in silicon to a depth of 900 nm.

Future work will focus on exploring issues related to coupling light into and out of the superprism. Some modifications of the current design will need to be made in the future to allow light to enter the device, excite the photonic crystal, and exit the device more effectively.

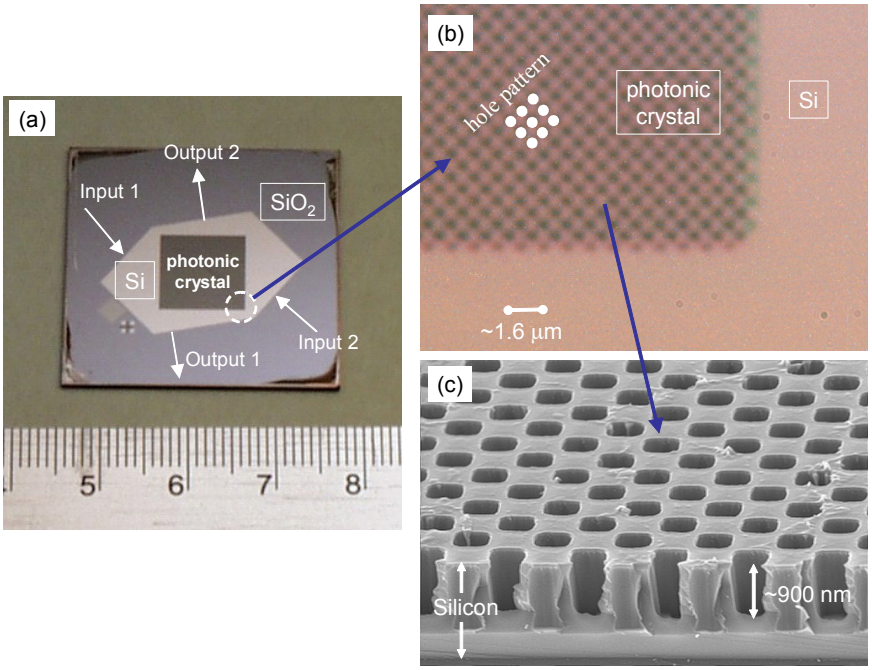

Figure 14. Images of fabricated superprism device. (a) Digital photograph showing full sample. (b) Nomarski Differential Interference Contrast image showing magnified corner area of the photonic crystal. (c) SEM micrograph showing cross-sectional image of a Si monitor sample.

7. Optical Nano-Mechanics

Sponsors:
National Science Foundation Award Number DMR-02-13282

Project Staff
Reginald E. Bryant, Solomon Assefa, Peter Rakich, Michelle L. Povinelli, Dr. Steven G. Johnson, Dr. Gale S. Petrich, Professor Erich P. Ippen, Professor John D. Joannopoulos, and Professor Leslie A. Kolodziejski

One major objective of optical engineering research is to bring optical systems to the large-scale functionality of electrical systems. Striving to reach this objective, a variety of optical devices are currently being developed in III-V material. Presently, focus has been set upon the deployment of nanometer-sized electromechanical-actuated waveguide devices with the prospect of broadening the functionality of integrated optical systems. These devices are termed optical NanoElectroMechanical devices (NEM devices).

The concept behind the NanoElectroMechanical high-index-contrast planar waveguide evanescent coupler switch combines two ideas to implement a new approach to transparent optical switching: high-index-contrast waveguide optics and electromechanical actuation. High-index-contrast waveguide optics are able to route optical energies through waveguides on 100-nanometer length scales (scaled in accordance to the operating wavelength). Directly following, the evanescent method of energy transfer occurs along 100-nanometer coupling lengths and separations. This leads to a small device-footprint, which lends itself to large-scale integrated switch optics. The physical dimensions of a high-index-contrast evanescent coupling provides for the development of planar NEM systems. Much like planar MicroElectroMechanical (MEM) systems, NEM systems benefit from mature silicon processes, making them relatively inexpensive to design and fabricate. Furthermore, due to the reduced dimensions of the NEM systems, it is possible to design switches with microsecond response times. Such response times open up a wider application space for this device that is not availed to larger MEM-based switch systems.

A considerable amount of design and fabrication work has been invested in the development of the NEMS switch. Figure 15 illustrates the operation of the ONEM switch. In the initial state with no applied voltage [Figure 15 (a)], the waveguides will be separated a distance of g_o defined by electron beam lithography. The initial distance of g_o is set so as to allow for propagation down the input waveguide with no lateral coupling to the adjacent waveguide. A potential difference is then applied to both waveguides [Figure 15(b) - (d)], which then reduces the separation of the two waveguides from g_o to a distance that will allow lateral coupling, g_{couple}. Figure 15(d) depicts the final deflected state where 100% of the optical energy is transferred from the initial waveguide to the adjacent waveguide.

Figure 16 represents the experimental product of a several-step fabrication sequence that involved two masking steps. Release lengths over 30 microns were achieved for fixed-beam waveguides with a 1-micron thickness and a width of approximately 300-nanometer.

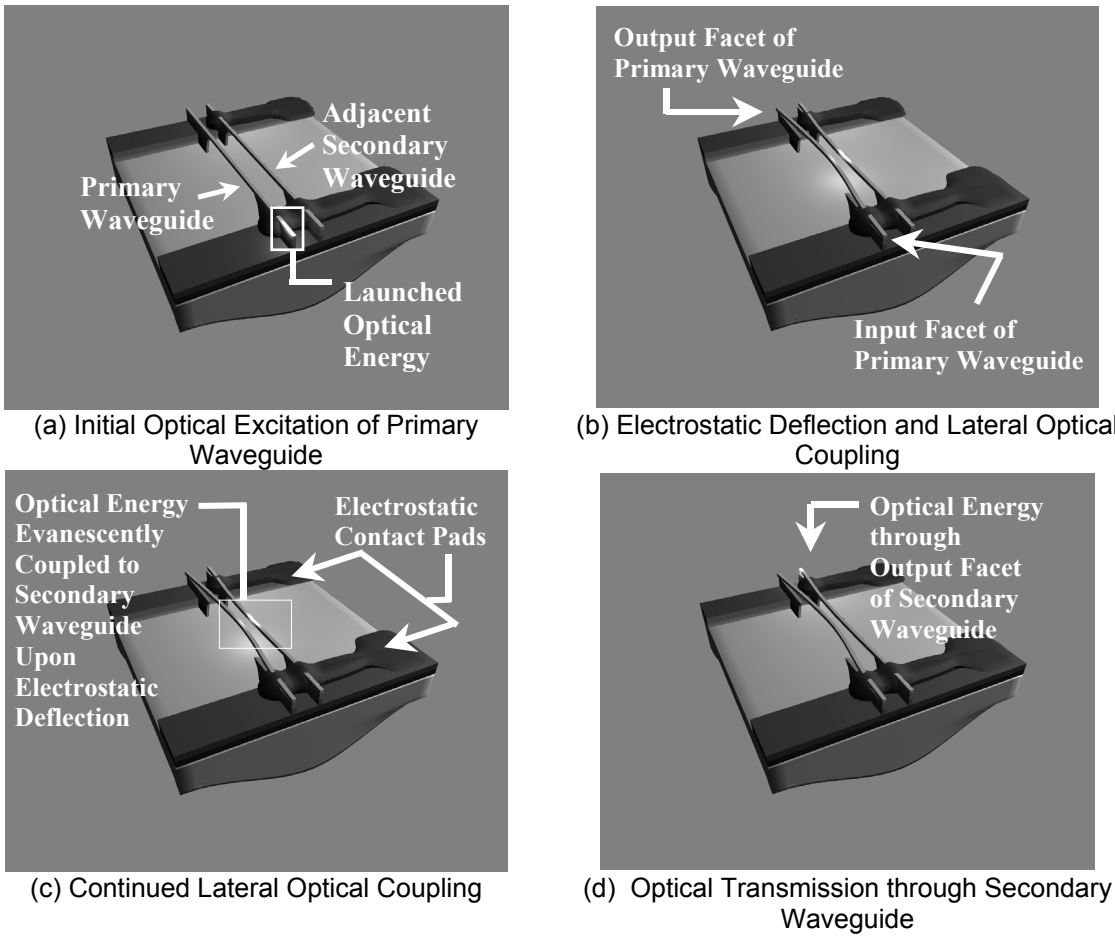

(a) Initial Optical Excitation of Primary Waveguide

(b) Electrostatic Deflection and Lateral Optical Coupling

(c) Continued Lateral Optical Coupling

(d) Optical Transmission through Secondary Waveguide

Figure 15. Four step diagram of proposed operation for the dual double clamped ONEM design

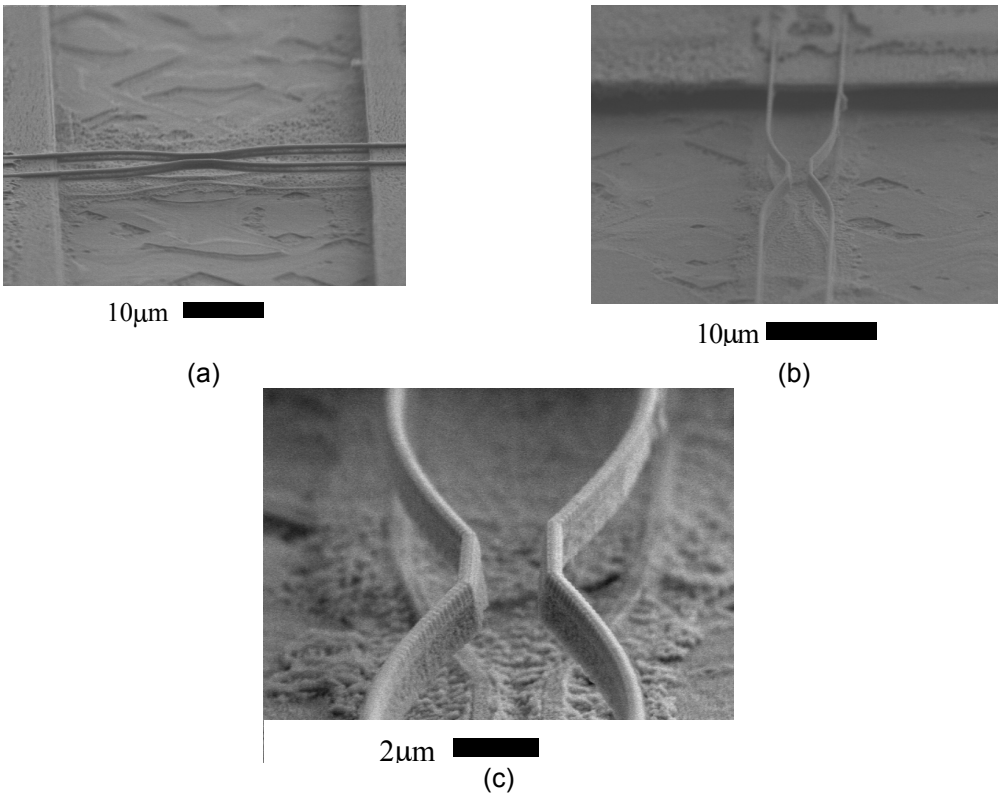

Figure 16. Scanning Electron Micrographs of a fabricated ONEMS device with an exponentially tapered geometry. (a) SEM slanted side view. (b) SEM slanted side view. (c) SEM close up of image b.

7. Photonic Devices in the Red Regime

Sponsors:
National Science Foundation Award Number DMR-02-13282
DARPA/Brown University Sub Award Number 1123-25496

Project Staff
Yamini Kangude, Solomon Assefa, Dr. Gale S. Petrich, and Professor Leslie A. Kolodziejski

A red emitting device at 650nm for use in a photonic crystal red light emitting diode was designed and fabricated. The design consisted of an active region where emission took place and a Bragg reflector. The active region utilized an $In_{0.5}Ga_{0.5}P$ quantum well and $In_{0.5}(Ga_{0.3}Al_{0.7})_{0.5}P$ cladding layers. The Bragg mirror was composed of seven bilayers of $In_{0.5}(Ga_{0.3}Al_{0.7})_{0.5}P$ and Al_xO_y. The device was grown by gas source molecular beam epitaxy. The mirror was fabricated by first depositing alternate layers of InGaAlP and AlAs and then oxidizing the AlAs layers to form Al_xO_y. Photoluminescence measurements showed that emission at 650nm was achieved.

A second red emitting device at 690nm was fabricated for use in an integrated organic-inorganic red emitter in conjunction with Brown University. The device was designed to pump the J-aggregate dye that was used as the organic material in the hybrid emitter. The design consisted of an active region composed of multiple quantum wells and a Distributed Bragg Reflector (DBR) beneath the active region. The multi-quantum well structure consisted of 8nm thick $In_{0.5}Ga_{0.5}P$ quantum wells and 5nm thick barriers of $In_{0.5}Ga_{0.28}Al_{0.22}P$. This structure was clad with 30nm thick layers of $In_{0.49}(Ga_{0.3}Al_{0.7})_{0.51}P$. The DBR that is designed to reflect at 690nm consisted of 16 bilayers composed of $Al_{0.4}Ga_{0.6}As$ and AlAs. The device

was grown by gas source MBE. Photoluminescence measurements showed that some overlap between the emission spectra and the absorption spectra of the J aggregate dye was achieved.

Publications

Journal Articles, Published

M. Povinelli, R. Bryant, S. Johnson, J. D. Joannopoulos, S. Fan, A. Erchak, E. Lidorikis, E. P. Ippen, G. S. Petrich "Design of a Nano-Electromechanical, High-Index-Contrast Guided-Wave Optical Switch for Single-Mode Operation at 1.55μm," IEEE Photonics Technology Letters. V 15 n 9, p. 1207 - 1209 (2003)

T. R. Schibli, J. Kim, O. Kuzucu, J. T. Gopinath, S. N. Tandon, G. S. Petrich, L. A. Kolodziejski, J. G. Fujimoto, E. P. Ippen, F. X. Kaertner, "Attosecond active synchronization of passively mode-locked lasers by balanced cross correlation" Optics Letters, v 28, n 11, p 947-9 (2003).

P. Bienstman, S. Assefa, S.J. Johnson, J.D. Joannopoulos, G.S. Petrich, and L.A. Kolodziejski "Taper Structures for Coupling into Photonic Crystal Slab Waveguides," Journal of the Optical Society of America B (Optical Physics), v 20, n 9, p1817-21 (2003).

Journal Articles, Submitted

S. N. Tandon, J. T. Gopinath, A. A. Erchak, G. S. Petrich, L. A. Kolodziejski, and E. P. Ippen. "Large Area Oxidation of AlAs Layers for Dielectric Stacks and Thick Buried Oxides." Accepted for Journal of Electronic Materials, February 2004.

Meeting Papers, Published

S. N. Tandon, J. T. Gopinath, T. R. Schibli, G. S. Petrich, L. A. Kolodziejski, F. X. Kaertner, and E. P. Ippen. "Saturable Absorbers with Large Area Broadband Bragg Reflectors for Femtosecond Pulse Generation." Lasers and Electro-Optics, 2003. CLEO '03. Technical Digest. Summaries of Papers Presented at the, CWM5 (2003).

T. R. Schibli, J.-W. Kim, L. Matos, A. W. Killi, J. T. Gopinath, G. S. Petrich, S. N. Tandon, L. A. Kolodziejski, E. P. Ippen, and F. X. Kaertner. "300-attosecond active synchronization of passively mode-locked lasers using balanced cross-correlation." Lasers and Electro-Optics, 2003. CLEO '03. Technical Digest. Summaries of Papers Presented at the, JTuC4 (2003).

S. Assefa, P. Bienstman, P. Rakich, S.J. Johnson, J. D. Joannopoulos, G. S. Petrich, L. A. Kolodziejski, E. P. Ippen, "Coupling into Photonic Crystal Slab Waveguides" Lasers and Electro-Optics, 2003. CLEO '03. Technical Digest. Summaries of Papers Presented at the, JWB1 (2003).

P. Rakich, S. Fan, A. A. Erchak, D. J. Rippin, G. S. Petrich, J. D. Joannopoulos, L. A. Kolodziejski and E. P. Ippen, "Efficient Coupling of Radiation into Guided Slab Resonances Through Two-Dimensional Photonic Crystal" Lasers and Electro-Optics, 2003. CLEO '03. Technical Digest. Summaries of Papers Presented at the, JWC1 (2003).

Meeting Papers, Submitted

S.N. Tandon, J.T. Gopinath, H.M. Shen, G.S. Petrich, L.A. Kolodziejski, F.X. Kaertner, and E.P. Ippen. "Broadband Saturable Bragg Reflectors from the Infrared to Visible using Oxidized AlAs." Accepted for Conference on Lasers and Electro-Optics (CLEO), 2004.

J.W. Sickler, J.T. Gopinath, S.N. Tandon, H. Sotobayashi, G.S. Petrich, E.P. Ippen, and L.A. Kolodziejski. "Femtosecond laser using broadband erbium-doped bismuth oxide gain fiber." Accepted for Conference on Lasers and Electro-Optics (CLEO), 2004.

S. Assefa, P. Rakich, P. Bienstman, S. G. Johnson, J. D. Joannopoulos, G. S. Petrich, L. A. Kolodziejski, E. P. Ippen and H. I. Smith, “Waveguiding in Photonic Crystals Consisting of Dielectric Pillars near 1550 nm” Accepted for Conference on Lasers and Electro-Optics (CLEO), 2004.

S. Assefa, G. S. Petrich, L. A. Kolodziejski, P. Rakich, I. P. Ippen, M. K. Mondol, and H. I. Smith, “Fabrication of Photonic Crystal Waveguides Composed of a Square Lattice of Dielectric Rods” Accepted for 48th International Conference on Electron, Ion, and Photon Beam Technology and Nanofabrication (2004)

H. Sotobayashi, J. T. Gopinath, E. M. Koontz, L. A. Kolodziejski and E. P. Ippen, “Wavelength Tunable Passively Modelocked Bismuth Oxide-based Erbium-doped Fiber Laser” Accepted to Optics Communications (2004).

References

[1] S.R. Forrest, M.R. Gokhale, P.V. Studenkov, Fengnian Xia, “Integrated photonics using asymmetric twin-waveguide structures”, Indium Phosphide and Related Materials, 2000. Conference Proceedings. 2000 International Conference on (2000) 13-16.

[2] P.V. Studenkov, M.R. Gokhale, S.R. Forrest, “Efficient coupling in integrated twin-waveguide lasers using waveguide tapers”, IEEE Photonics Technology Letters, Vol. 11, n. 9 (1999) 1096-1098.

[3] Z. Zhang, T. Nakagawa, K. Torizuka , T. Sugaya, K. Kobayashi, "Gold-reflector-based semiconductor saturable absorber mirror for femtosecond mode-locked Cr4+:YAG lasers," Applied Physics B, **70**, S59, 2000.

[4] M. Haiml, L. Gallmann, U. Keller, "GaAs absorber layer growth for broadband AlGaAs/fluoride SESAMs" Journal of Crystal Growth, **227-228**, 172, 2001.

[5] T. R. Schibli, J. Kim, O. Kuzucu, J. T. Gopinath, S. N. Tandon, G. S. Petrich, L. A. Kolodziejski, J. G. Fujimoto, E. P. Ippen, and F. X. Kaertner. "Attosecond active synchronization of passively mode-locked lasers by balanced cross correlation." *Optics Letters*, **28** (2003) 947.

[6] J.W. Sickler, J.T. Gopinath, S.N. Tandon, H. Sotobayashi, G.S. Petrich, E.P. Ippen, and L.A. Kolodziejski. "Short-pulse laser using erbium-doped bismuth oxide fiber." Submitted to Conference on Lasers and Electro-Optics (CLEO), 2004.